

1 Introduction

1.1 General Overview

Cross-flow-induced vibration of bluff bodies, i.e. bodies whose aspect is not small compared with the streamwise dimension, are ubiquitous, in nature as well as in man-made constructions. The wind-induced fluttering of leaves and tree branches and the waving motions in wheat fields are examples of the former. The Aeolian harp, going back perhaps 3000 years, is an example of the earliest realization and/or exploitation of the existence of these vibrations made by man.

Perhaps the first documented and surviving realization of the existence of vortex shedding as such goes back to two Renaissance paintings in Bologna and a sketch by Leonardo da Vinci, thus, to the 14th and 15th centuries.* The modern study of vortex shedding began in the late 19th century, with Strouhal (1878), Bénard (1908) and von Kármán (1912). Studies on vortex-induced vibrations followed soon after; lock-in, or shedding frequency synchronization, was first documented by Bishop & Hassan (1964).

With such a venerable and long pedigree, it is not surprising that the topic of cross-flow-induced vibrations and instabilities of bluff bodies, notably cylinders or groups of cylinders, is truly vast. To make any headway in this topic, one must first understand the fluid mechanics of the flow around bluff bodies, while stationary or in motion, and the forces generated thereon. Because these depend on the Reynolds number, roughness, flow confinement, aspect ratio, amplitude of motion and many other factors, the task of documenting, categorizing and making sense of the voluminous amount of research done over the past 100 years or so is truly Herculean. In this regard, one must pay tribute to the excellent work done by Zdravkovich (1997, 2003); the task is so huge that the work covered in the first two volumes already published, involving 1264 pages, has not yet reached the point of considering

* One painting from the end of the 14th century, attributed to Giovanni da Modena and found in Bologna, depicts the Christ-bearing (*Χριστόφορος*) San Cristoforo crossing a stream and shows an alternating pattern of vortices downstream of his legs (Tokaty 1971; Sumner 1999). Another, entitled *Madona col Bambino tra i Santo Domenico, Pietro Martire e Cristoforo* is a 15th-century mural in the Basilica de San Domenico in Bologna, again showing vortices from the foot of St. Christopher crossing a stream (von Kármán 1954; Zdravkovich 2003). The drawing by Leonardo da Vinci from roughly the same period shows vortices in the wake of a pile in a stream (Lugt 1983; Blevins 1990; Zdravkovich 1997; Mizota *et al.* 2000).

fluid-coupled, self-excited motions. The difficulty of this task is exacerbated by the fact that, routinely, for decades now, there is hardly an issue of the *Journal of Fluid Mechanics* or the *Journal of Fluids and Structures*, or indeed the *Journal of Sound and Vibration*, the *Journal of Wind Engineering and Industrial Aerodynamics* or the *Journal of Fluids Engineering*, without one or several papers related to cross-flow about bluff bodies, the forces and motions induced thereby and so on. Thus, it is not only that the accumulated knowledge is vast, but also that the accretion of knowledge and experience on the topic continues to grow unabated, perhaps exponentially.*

Of course, other books exist in which chapters may be found on cross-flow-induced vibrations and instabilities, published over the past 25 years: by Blevins (1977, 1990), Sarpkaya & Isaacson (1981), Chen (1987), Naudascher & Rockwell (1994, 2005), Gibert (1998), Sumer & Fredsøe (1997), Au-Yang (2001), Axisa (2001), de Langre (2001), Kaneko *et al.* (2008) and others. However, these books cover several topics other than cross-flow-induced vibrations and instabilities, and in Zdravkovich (1997, 2003) and the forthcoming Volume 3 of that work it is attempted to cover the whole field of cross-flow about bluff bodies. In contrast, the present book is more modest in scope and its aim more focussed.

In this book, the focus is on the interaction of the cross-flow with motions of the bluff structure, presuming that the flow field and the forces associated with prescribed motions of the structure are known *a priori*. Furthermore, the vista is further limited by excluding extraneously induced excitation (EIE) and instability-induced excitation (IIE) in Naudascher & Rockwell's (1980, 1994) classification of flow-induced oscillation phenomena. The subject matter in this book is therefore broadly associated with *movement-induced excitation* (MIE) phenomena, in which the excitation is intimately coupled with, indeed caused by, movements of the body. Hence, the phenomena are *self-excited*. In the linear sense, these phenomena are *instabilities*; i.e., as a parameter is incremented, a system hitherto in a quiescent state becomes subject to self-excited oscillation – as discussed further in Section 1.2. Hence, the topic is: *self-excited oscillations involving bluff bodies in cross-flow*.†

Why so much interest in bluff-body/flow interactions, indeed, in the subject of this book? The immediate answer is that (i) bluff bodies, in particular, cylinders and prisms, are ubiquitous in engineering structures, typically as components of larger systems; (ii) in many cases these bluff bodies are subjected to flow (cross-flow); and (iii) frequently problems arise, often in the form of self-excited oscillations, the solution if not prevention of which necessitates understanding the fluid-structure interaction mechanisms involved. Every engineering student learns about the Tacoma Narrows Bridge disaster and may have seen the spectacular ciné-film of its collapse. However, apart from bridges, cross-flow-induced vibrations occur in (i) heat exchangers and other power-generation components; (ii) offshore structures, including risers and submerged pipelines; (iii) high-rise buildings, silos and chimneys;

* In this respect, one has to marvel at Mickey Zdravkovich's tenacity. As he has told the first author, the main difficulty in writing his books was that, no sooner was a particular chapter closed and the writing progressed to the next and subsequent ones, that it had to be reopened because interesting and pertinent new information had been published in the meantime. And, of course, one cannot cry "stop!" anymore than one can ignore the new knowledge.

† Here, of course, the definition of "bluff-bodies in cross-flow" is pleonastic, just as "slender body in axial flow" is; however, the redundancy enhances the clarity of the definition.

1.2 Concepts and Mechanisms

3

(iv) overhead transmission lines and cables; and within (v) fluid-manipulating machinery in mechanical and chemical plants, to give but a partial list. Thus, the flows involved are either contained gas or liquid flows, or generally unconfined flows due to wind and water currents.

In the long list of engineering applications just mentioned, “problems” arise associated with self-excited oscillations or cross-flow-induced instabilities. These problems range from short-term destruction of the structure to unacceptable long-term wear (fretting) problems and fatigue. Some examples may be found in Paidoussis (1980, 2006), Axisa (1993), Au-Yang (2001) and Kaneko *et al.* (2008). Many of these are related to the power-generating industry, in particular, to nuclear plants, where disclosure of all types of problems, including flow-induced problems, is mandatory in many states. Other incidents, however, remain hidden from public view, their existence being surmised only by sudden upsurges in research funding; or, at the very least, they are incompletely reported,* e.g. in the offshore industry.

It is opportune to contrast the research on cross-flow-induced instabilities to that on axial-flow-induced ones. In the latter, much, though by no means all, of the research work was curiosity-driven (Paidoussis 1998, 2004), with many of the applications emerging 10 or 20 years later (Paidoussis 1993). For cross-flow, on the other hand, much work was inspired by, or necessitated for, concrete applications. This reflects the fact that, with the exception of some classes of axial-flow-induced vibration, notably involving annular and leakage flows, catastrophic failure is rather rare. For cross-flow situations, however, problems have abounded and are not all that rare even today. In one subtopic alone, that of fluidelastic instabilities of cylinder arrays in cross-flow, the cumulative damages incurred over a decade were estimated at 1000 M\$ (Paidoussis 2006).

Something that ought to be stressed is that flow-induced vibrations of structures subject to cross-flow are inevitable and often innocuous. It is only when the amplitudes become large enough, as is often the case with flow-induced instabilities, that they become worrisome. The main task of this book is to elucidate the mechanisms underlying these instabilities and to provide means for predicting their occurrence.

It should also be pointed out that flow-induced vibrations and instabilities are not always undesirable. For instance, naturally occurring flow-induced vibrations help in promoting the dispersion of plant seeds (de Langre 2008). In addition, they can be exploited for engineering purposes, e.g. in ocean-current-driven energy-harvesting devices.

As stated in the Preface, it is here emphasized that the treatment in this book is not exhaustive. Rather, the emphasis is very much on the fundamentals and on a physical understanding of the mechanisms involved to the extent possible. Beyond that, a full list of references guides the reader to the available literature in each subtopic.

1.2 Concepts and Mechanisms

The purpose of this section is to clarify some of the terms and concepts referred to in the foregoing and used extensively in this book, e.g. the concepts of instability

* Mainly to protect the corporate image on a trade mark, or for fear of litigation.

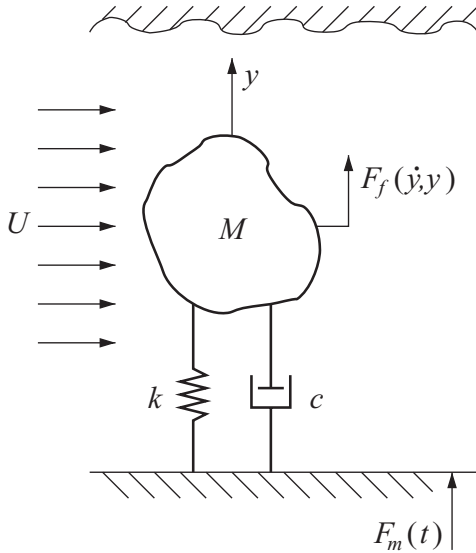


Figure 1.1. A flexibly supported bluff body of mass $M \equiv ml$ in cross-flow.

and self-excited vibrations, in the process clarifying also some of the underlying mechanisms.

1.2.1 Self-excited oscillations and instabilities

The truth about self-excited oscillations is that they are not truly self-excited. That is, a mechanical system does not by itself spontaneously break into oscillation, unless the definition of the system includes the source of energy, e.g. a fluid flow, which is responsible for the oscillation (Den Hartog 1956, chapter 7; Magnus 1965, chapter 3). As we shall see, however, the governing equation of motion may be written in a way that the resulting oscillation *appears* to be self-excited.

Consider, for example, a flexibly supported bluff body which could be modelled as a mass-dashpot-spring system, as shown in Figure 1.1, free to move in the direction transverse to the flow; the cross-section of the body is uniform along its length l (normal to the plane of the paper), so that its total mass $M = ml$, where m is the mass per unit length. The bluff body is subjected to a fluid-dynamical force $F_f(\dot{y}, y)$, as well as a mechanical force $F_m(t)$, e.g. a base excitation; y is the transverse displacement and \dot{y} the corresponding velocity. Thus, we have

$$m\ddot{y} + c\dot{y} + ky = F_f(\dot{y}, y) + F_m(t), \quad (1.1)$$

where the overdot denotes differentiation with respect to t . Here, l is assumed to be sufficiently large for the flow around the body to be sensibly two-dimensional. Suppose further that F_f may be expressed as $\frac{1}{2}\rho U^2 h l C_{f1}(\dot{y}, U) + \frac{1}{2}\rho U^2 h l C_{f2}(y, U)$, where h is a characteristic length (typically the diameter for a cylindrical body, or the frontal height of the cross-section *vis-à-vis* the flow), and C_{f1} and C_{f2} are fluid-dynamic force coefficients, respectively functions of \dot{y} and y , and weakly of the mean flow velocity U . Velocity dependence may arise because the instantaneous angle of attack of the flow on the body as the body oscillates is $\theta = \tan^{-1}(\dot{y}/U)$. Position dependence may arise through proximity of the bluff body to, say, a wall, so that the

1.2 Concepts and Mechanisms

5

fluid forces depend on the distance from the wall. In equation (1.1), it is presumed that $m = m_s + m_a$, m_s being the structural mass and m_a the added or virtual fluid-dynamic mass per unit length. For an oscillating body, the acceleration-related pressure field gives rise to a force which may be written as $m_a l \ddot{y}$, thus defining m_a ; for a dense fluid, m_a/m_s is not negligible (e.g., for a circular cross-section, $m_a = \rho(\pi/4)D^2$ according to potential flow theory, D being the diameter) – see Section 3.4.1. Thus, this could have been incorporated in (1.2) as a third fluid-dynamical force, linearly dependent on \ddot{y} and independent of U , while taking $m = m_s$.

Succinctly, the difference between F_f and F_m is that for $y = 0$ and $\dot{y} = 0$, F_f will be zero (or a constant force that can be eliminated by a change of variable from y to $y^* = y - y_0$). Thus, writing the equation in terms of y^* and suppressing the asterisk, we have

$$m l \ddot{y} + c \dot{y} + k y = \frac{1}{2} \rho U^2 h l C_{f_1}(\dot{y}, U) + \frac{1}{2} \rho U^2 h l C_{f_2}(y, U) + F_m(t), \quad (1.2)$$

where it is understood that if $y = 0$, $\dot{y} = 0$, the first two forcing functions (representing $F_f(\dot{y}, y)$) vanish; thus, they only arise because of motion, whereas $F_m(t)$ is not affected by the motion. Having served to clarify the distinction between itself and F_f , we shall from now on ignore $F_m(t)$.

We can next write equation (1.2) in dimensionless form by defining $c/ml = 2\zeta\omega_n$ and $k/ml = \omega_n^2$, as well as

$$\eta = y/l, \quad \tau = \omega_n t, \quad U_r = U/(\omega_n h), \quad \mu_r = \rho h^2/m, \quad (1.3)$$

where U_r is the so-called *reduced flow velocity* and μ_r is a *mass ratio*, obtaining*

$$\ddot{\eta} + 2\zeta\dot{\eta} + \eta = \frac{1}{2}\mu_r U_r^2 C_{f_1}(\dot{\eta}, U_r) + \frac{1}{2}\mu_r U_r^2 C_{f_2}(\eta, U_r), \quad (1.4)$$

where the overdot is now $d(\)/d\tau$. It is assumed next, for simplicity, that C_{f_1} may be expressed as a function of $\dot{\eta}/U_r$ and C_{f_2} as a function of η alone. For the purposes of this illustrative example, let

$$\frac{1}{2}\mu_r U_r^2 C_{f_1}(\dot{\eta}, U_r) = \beta_1(U_r)\dot{\eta} - \beta_3(U_r)\dot{\eta}^3, \quad \frac{1}{2}\mu_r U_r^2 C_{f_2}(\eta, U_r) = \gamma_1(U_r)\eta - \gamma_3(U_r)\eta^3,$$

and hence equation (1.4) is written as

$$\ddot{\eta} + [2\zeta - \beta_1(U_r) + \beta_3(U_r)\dot{\eta}^2]\dot{\eta} + [1 - \gamma_1(U_r) + \gamma_3(U_r)\eta^2]\eta = 0. \quad (1.5)$$

Thus, at first glance, considering the quantities in square brackets as an effective damping and an effective stiffness, the source of energy input in this autonomous system is “hidden”.

Let us further assume that β_1 , β_3 , γ_1 and γ_3 are positive, monotonically increasing functions of U_r in view of the weak dependence of C_{f_1} and C_{f_2} on U_r , and let us consider the dynamics displayed by equation (1.5).

First, taking $\gamma_1 = \gamma_3 = 0$ for the moment, it is clear that for arbitrarily small $|\dot{\eta}|$ the dynamics is controlled by the linear terms and hence by the sign of $2\zeta - \beta_1$: if it is positive, as it must be for sufficiently small U_r , the damping is positive and the oscillations will be damped; for higher U_r , however, it becomes negative, which

* Equation (1.4) holds true also if equation (1.1) is written in two-dimensional or “sectional” form. In that case, m would replace ml in equation (1.2); similarly, k and c could represent distributed quantities per unit length, or the total acting on the bluff body divided by l ; also, l would be absent from the right-hand side of (1.2). Equations (1.3) would be the same.

means *negative damping* and *self-excited oscillations*. Thus, the threshold of linear instability of the system, U_{rc} , occurs at $\beta_1(U_{rc}) = 2\zeta$; according to linear theory, the amplitude of the self-excited oscillation will grow indefinitely. However, taking the $\beta_3(U_r)\dot{\eta}^3$ term into account, it is clear that for sufficiently large $|\dot{\eta}^3|$, the damping ceases to be negative; indeed, the quantity in square brackets becomes zero on the average, and one obtains *limit-cycle oscillation*. Thus, the growth of amplitude is self-limiting. In this case, the limit cycle is stable, as both positive and negative increments (perturbations) to $\dot{\eta}$ are damped, returning the system to the limit cycle; the case of an unstable limit cycle is discussed later.

From the nonlinear perspective, the linear threshold of instability is referred to as a *bifurcation*, leading in this case from one stable state, the trivial equilibrium, to another stable state, the limit-cycle oscillation. However, in engineering terms, the linear threshold of instability at U_{rc} is commonly called the threshold of instability, regardless.

Bifurcation has a broader meaning than for the situation just discussed: it is associated with any qualitative change in the state or dynamical behaviour of a system, e.g. from periodic to quasiperiodic oscillation, or from quasiperiodic to chaotic.

Let us next consider the statics of the system, clearly governed by the last term of equation (1.5). For small $|\eta|$, the effective linear stiffness, $1 - \gamma_1(U_r)$, is positive, provided U_r is sufficiently small; for any small departure from $\eta = 0$, the stiffness force restores the original static equilibrium. For higher U_r , however, we may have a *negative stiffness*, $1 - \gamma_1(U_r) < 0$, leading to static instability, a *static divergence*, implying a nonoscillatory amplification, without limit, of any small departure from the now unstable trivial equilibrium. Taking the nonlinear term into account, however, it is clear that two new equilibria are born for sufficiently large $|\eta|$: at $\eta_{st} = \pm\{[1 - \gamma_1(U_r)]/\gamma_3(U_r)\}^{1/2}$, which may, in general, be stable or unstable (in the sense of the equilibria of a pendulum at $\theta = 0$ and π , respectively) – but for the form of the stiffness term here always unstable.

The dynamics of the system of equation (1.5) could be displayed as a three-dimensional plot of $(\eta, \dot{\eta}, U_r)$. Any “cut” thereof along the U_r -axis would yield a phase-plane plot $(\eta, \dot{\eta})$. To make things more interesting and instructive, we henceforth relax the requirement that $\beta_3(U_r)$ and $\gamma_3(U_r)$ be positive. Thus, consider the system at $U_r = U_{r1}$, such that equation (1.5) becomes

$$\ddot{\eta} - 0.02(1 - \dot{\eta}^2)\dot{\eta} + (0.95 - 0.018\dot{\eta}^2)\eta = 0. \quad (1.6)$$

In view of the foregoing, this represents a system just beyond the onset of linear self-excited oscillation; i.e. here $2\zeta - \beta_1(U_{r1}) = -0.02$, while $\beta_3(U_{r1}) = 0.02$. Also, $1 - \gamma_1(U_{r1}) = 0.95$ and $\gamma_3(U_{r1}) = -0.018$.

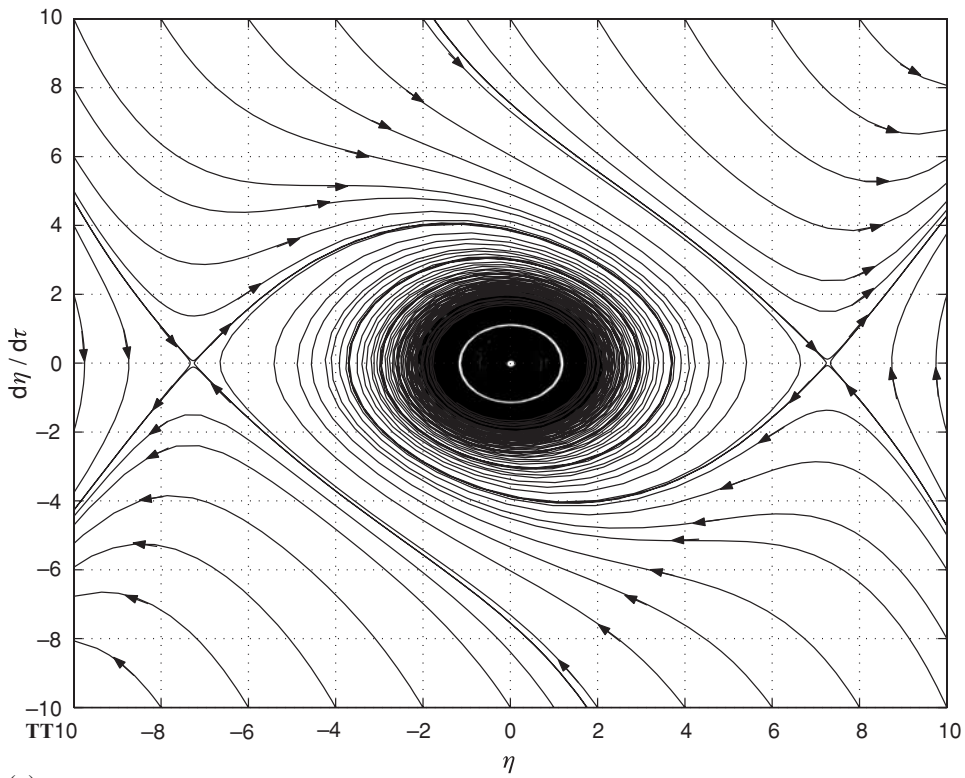
The dynamics is displayed in Figure 1.2(a). It is seen that the origin (trivial equilibrium) is unstable, and that a stable limit cycle exists at $|\eta| \simeq 1.1$ (the oval region purposely left blank for clarity). Trajectories for $|\eta| < 1.1$ and $|\eta| > 1.1$ but not too far away, spiral outwards and inwards, respectively, towards the limit cycle. There are also two new *fixed points*, i.e. points of static equilibrium, at $|\eta| = (0.95/0.018)^{1/2} \simeq 7.26$. They are unstable; specifically, they are *saddle points*. In this case, the *basin of attraction* of the limit cycle is the diagonal swath from the upper left of the figure to the lower right, within the area delimited by the trajectories going through the saddle points.

Cambridge University Press

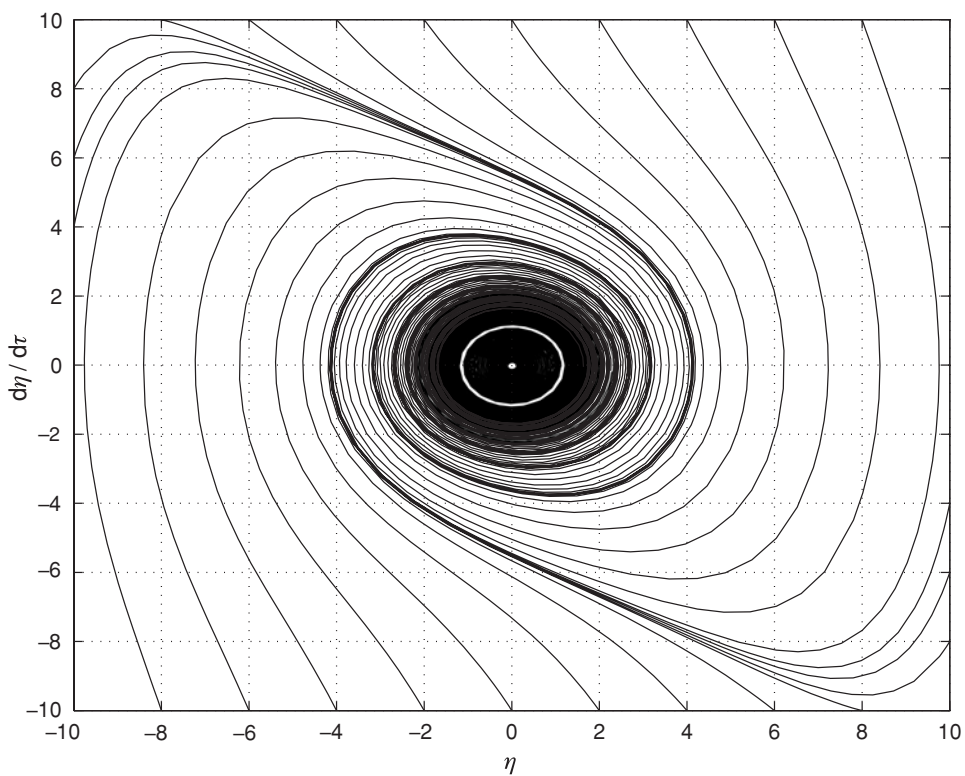
978-0-521-11942-9 - Fluid-Structure Interactions: Cross-Flow-Induced Instabilities

Michael P. Paidoussis, Stuart J. Price and Emmanuel de Langre

Excerpt

[More information](#)

(a)



(b)

Figure 1.2. Phase-plane diagrams for the system of equation (1.4) for different system parameters: (a) for the system $\ddot{\eta} - 0.02(1 - \dot{\eta}^2)\dot{\eta} + (0.95 - 0.018\eta^2)\eta = 0$; (b) for the system $\ddot{\eta} - 0.02(1 - \dot{\eta}^2)\dot{\eta} + (0.95 + 0.018\eta^2)\eta = 0$.

For $\gamma_3(U_{r1}) = +0.018$ in equation (1.5), i.e. when the equation of motion is

$$\ddot{\eta} - 0.02(1 - \dot{\eta}^2)\dot{\eta} + (0.95 + 0.018 \eta^2)\eta = 0, \quad (1.7)$$

the saddle points disappear, as shown in Figure 1.2(b), and the basin of attraction of the limit cycle covers the whole figure. Taking a global view of the dynamics, we can say that the system is *unstable in the small* (i.e. in the region within the limit cycle close to the origin), and *stable in the large*. In general, “small” and “large” are suggested by the physics of the system, but may be subjective.

For $\gamma_3(U_{r1}) = 0.018$ and $\beta_3(U_{r1}) = -0.02$, i.e. for the equation

$$\ddot{\eta} - 0.02(1 + \dot{\eta}^2)\dot{\eta} + (0.95 + 0.018 \eta^2)\eta = 0, \quad (1.8)$$

the stable limit cycle disappears also. This does not imply that the physical system is unstable at all nonzero amplitudes. It simply means that the nonlinear model of equation (1.8) is not accurate enough. A more accurate representation, e.g. involving a positive $\beta_5(U_{r1})\dot{\eta}^5$, could again give rise to a stable limit cycle (see, e.g., Paidoussis (1998, section 2.3)).

Next, consider the system of equation (1.5) at $U_{r2} < U_{r1}$, such that $2\zeta - \beta_1(U_{r2}) > 0$. The equation of motion is now

$$\ddot{\eta} + 0.02(1 + \dot{\eta}^2)\dot{\eta} + (0.95 + 0.018\eta^2)\eta = 0. \quad (1.9)$$

The limit cycle disappears and the trivial equilibrium becomes a stable fixed point.

Consider next another system, governed by

$$\ddot{\eta} + 0.02(1 - \dot{\eta}^2 + 0.05\dot{\eta}^4)\dot{\eta} + (0.95 - 0.018\eta^2)\eta = 0. \quad (1.10)$$

The phase-plane plot is shown in Figure 1.3. In this case the blank oval at $|\eta| \simeq 1.1$ is an *unstable* limit cycle, nesting within a stable limit cycle going through $|\eta| \simeq 6.2$. Thus, trajectories within the unstable limit cycle spiral towards the origin, and those on the outside spiral towards the stable limit cycle – as do trajectories outside the latter. This represents a not-too-rare system in practice: a system stable at the origin which if lightly perturbed will return to the origin; but, if strongly perturbed to beyond the unstable limit cycle, it will develop large-amplitude limit-cycle oscillations.

1.2.2 Argand diagrams and bifurcations

For an N -degree-of-freedom system or an N -mode discretization of a distributed parameter system, let the N dimensionless eigenfrequencies be denoted by ω_r and the eigenvectors by $\{A\}_r$, $r = 1, \dots, N$, and let the linear solution of the autonomous system be expressed as

$$\{q\} = \sum_{r=1}^N \{A\}_r e^{i\omega_r \tau}. \quad (1.11)$$

In general, $\omega_r = \mathcal{R}e(\omega_r) + i \mathcal{I}m(\omega_r)$. It is clear that if for one of the ω_r , say for ω_s , $\mathcal{I}m(\omega_s)$ is negative, the system is linearly unstable, since the solution will then involve a term $\exp(\alpha_s \tau)$, where $\mathcal{I}m(\omega_s) = -\alpha_s$ and $\alpha_s > 0$.

As one of the system parameters is varied, say the dimensionless flow velocity u , the evolution of the ω_r is often displayed as an Argand diagram, in which $\mathcal{I}m(\omega_r)$ is plotted versus $\mathcal{R}e(\omega_r)$ with u as parameter.

1.2 Concepts and Mechanisms

9

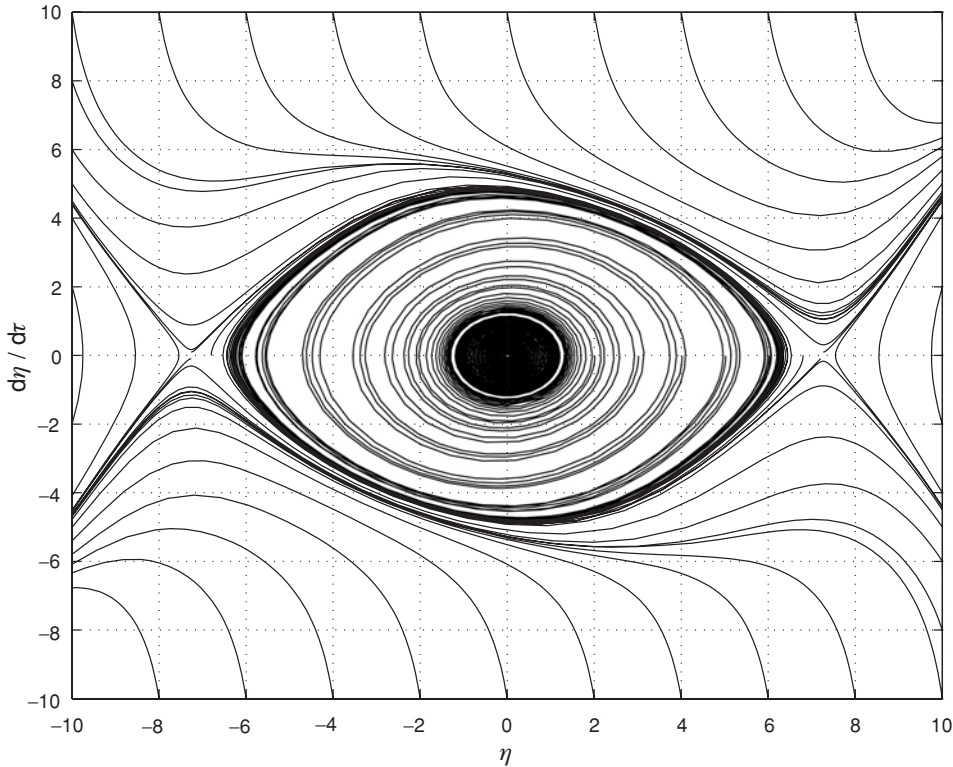


Figure 1.3. Phase-plane diagram for the version of the system of equation (1.4) described by $\ddot{\eta} + 0.02(1 - \dot{\eta}^2 + 0.05\dot{\eta}^4)\dot{\eta} + (0.95 - 0.018\eta^2)\eta = 0$.

Figure 1.4 shows such diagrams, illustrating several ways in which the frequency loci may cross from the stable $+\mathcal{I}m(\omega_r)$ half of the frequency plane to the unstable $-\mathcal{I}m(\omega_r)$ half.

Figure 1.4(a) shows the onset of *divergence* via a *pitchfork bifurcation** in the first mode of a conservative system. As ω_1 is purely imaginary for $u > u_c$, this is clearly a static instability.

Figure 1.4(b) illustrates loss of stability via *Hopf bifurcation* for a nonconservative system with zero structural damping ($\mathcal{I}m(\omega_2) = 0$ at $u = 0$). Clearly, as $\mathcal{R}e(\omega_2) \neq 0$ at $u = u_c$, this is an oscillatory instability, signifying *single-mode amplified oscillations* or *flutter*.

Flutter can also arise through coalescence of two modes in the form of *coupled-mode flutter*, as shown in Figure 1.4(c, d), again for systems with zero structural damping. The fact that the eigenfrequencies are purely real prior to instability is indicative of the system being conservative. The coupled-mode flutter displayed in Figure 1.4(c) is via a so-called *Hamiltonian Hopf bifurcation*.

In Figure 1.4(d) the loci of the modes lie either on the $\mathcal{R}e(\omega)$ or the $\mathcal{I}m(\omega)$ axis, but they are drawn just off the axes for clarity. The coupled-mode flutter in this case is via a *secondary bifurcation*, i.e. after the system has lost stability by divergence – in

* Strictly speaking, the type of bifurcation involved is defined by the nonlinear terms in the equation of motion. In this case, the flow-related nonlinearities in the stiffness term are cubic and similar to those in a softening cubic spring. This is what gives rise to two stable static equilibria for $u > u_c$.

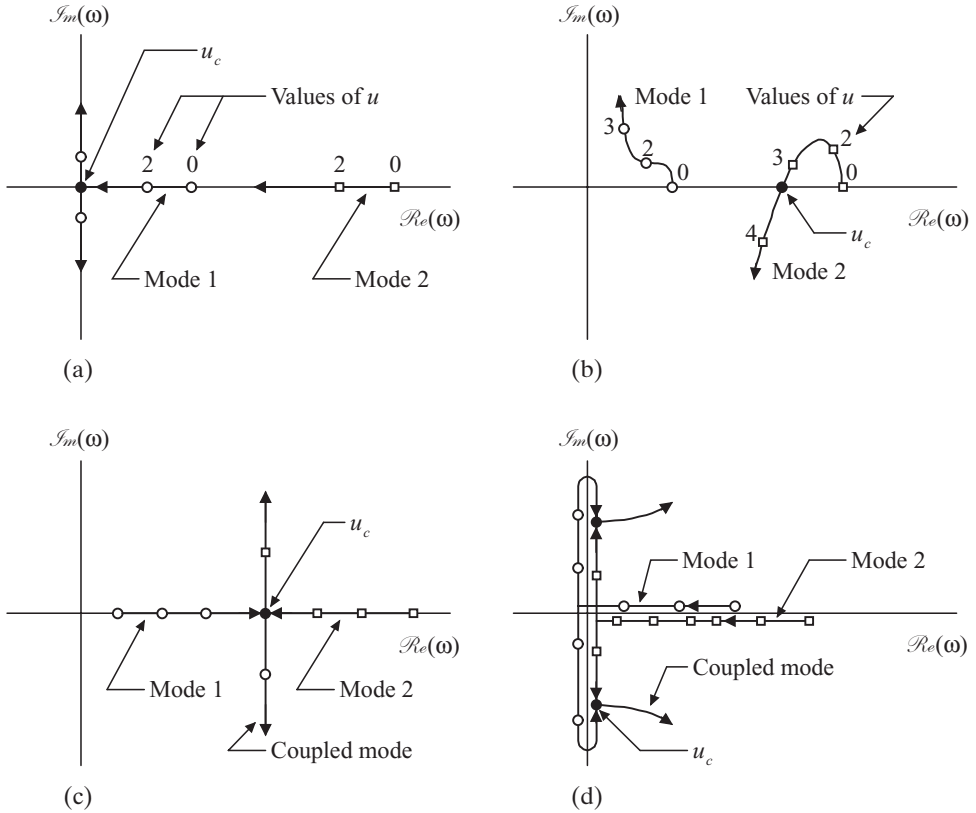


Figure 1.4. Argand diagrams illustrating loss of stability via (a) a pitchfork bifurcation of a conservative system, leading to static divergence, (b) a Hopf bifurcation of a nonconservative system, (c) a Hamiltonian Hopf bifurcation, leading to coupled-mode flutter, (d) a so-called Paidoussis coupled-mode flutter, all for nondissipative systems; u_c denotes the critical dimensionless flow velocity.

this case, in both the first and second modes.* To distinguish it from the Hamiltonian coupled-mode flutter, Done & Simpson (1977) christened it as *Païdoussis coupled-mode flutter*, because it was first documented in a paper by Païdoussis & Issid (1974); its principal characteristic is that, at onset, the frequency of oscillation is zero, but it becomes finite as u is increased.

It is instructive to consider how these bifurcations are affected by the presence of dissipative effects and nonlinearities. Figure 1.5 shows the effect of dissipation on the bifurcations. It is clear that the bifurcations in Figure 1.5(a, b) are not qualitatively different from those in Figure 1.4(a, b).

Figure 1.5(c) is distinctly different, however. The two modes nearly collide and then veer away from each other (*mode-veering* phenomenon), and one of them crosses the $\mathcal{R}e(\omega)$ -axis to the unstable domain; thus, the coupled-mode flutter devolves to a form of single-mode flutter. In a sense, something similar is shown in Figure 1.5(d), although the coupled-mode flutter in this case survives, but involves the coalescence of two branches of the first mode.

* Another form involves the coalescence of the two branches of the same mode [see, e.g., Païdoussis (1998, fig. 3.14); also Figure 1.5(d)].